Controlled Fabrication of Hydrogel Janus Microparticles Containing Opal Structures via Sequential Micromolding

A thesis submitted by

Michael DeCortin

In partial fulfillment of

of the requirements for the

Senior Honors Thesis

Undergraduate Chemical and Biological Thesis Program

at

The Department of Chemical and Biological Engineering

Tufts University

Thesis Committee Members:

Chair: Dr. Hyunmin Yi

Dr. James Van Deventer

2017

Abstract

Janus hydrogel microparticles containing synthetic opal structures formed via deposition of polystyrene beads have significant potential for reagentless detection of environmental monitoring and sensing of biomacromolecular binding events. However, there exist significant issues for the reliable and robust fabrication of such microparticles. This thesis tests important parameters for the tunable fabrication and characterization of these microparticles via a two-step sequential micromolding technique. Parameters examined are ethanol concentration, surfactant addition and concentration, polystyrene bead diameter for the opal structure layer, and both polyacrylamide and poly(ethylene glycol) diacrylate polymer systems for the hydrogel layer. I demonstrated that a poly(ethylene glycol) diacrylate system results in the reliable fabrication of microparticles with uniform and intense color. I developed a modified Bragg's equation that readily predicts structural color that agrees well with the experimental results. These studies show significant progress towards a greater understanding of opal structures formed via polystyrene bead deposition, and the robust and reliable fabrication of Janus hydrogel microparticles that have significant potential for biosensing applications in the future.

Table of Contents

List of Figures

List of Equations:

List of Tables:

1. Introduction:

Synthetic opal structures have been created from a variety of materials such as silica[1], polymers[2], or titanium[3] on the nanoscale level. When these materials are packed into a closely packed crystal structures, for example face centered cubic (FCC), they exhibit a photonic band gap.[4] A photonic band gap prevents most wavelengths from passing through the crystal structure which results in intense structural color. Opal structured materials hold significant potential for reagentless detection in applications such as biosensing or medical diagnostics, since binding events can lead to changes in the observed structural color which is governed by the Bragg's equation[5]. The Bragg's equation states that the photonic band gap is a function of the materials being used and the size of the crystal structures[6]. Synthetic opal structures have already been shown to have applications as soft materials in lasers[7], chemical sensors[8], and data storage[9].

Meanwhile, polymeric hydrogel microparticles also hold great potential in both biosensing applications and medical diagnostics. Hydrogels are crosslinked networks of hydrophilic polymers[10], and they are desirable for biosensing applications due to their rapid solution-like kinetics, non-fouling nature, rapid assay time, and tunable properites[10]. One of the most common fabrication techniques for hydrogels is utilization of microfluidics. Briefly, microfluidics cause the formation of hydrogels by varying two different laminar flows with different properties that cause surface-tension induced droplet formation followed by exposure to UV light[11]. However there are a number of issues with microfluidics such as the need for delicate microflow control, harsh processing conditions, requirement of rapid polymerization, and lack of scalability[12]. Hydrogel microparticles containing opal structures have been fabricated using microfluidics[13,14] and have been shown to change properties under various stimuli. However, due to the previously stated issues with microfluidics there still exists a need for consistent and

reproducible fabrication of intensely colored microparticles that are produced under mild conditions.

To combat the issues with microfluidics devices, micromolding techniques have been developed[10,12]. Micromolding offers a simple, robust, and scalable fabrication of polymeric microparticles[12]. In this thesis, I aim to fabricate hydrogel Janus microparticles via a two step-sequential micromolding technique that have intense and uniform color. The method utilized in this thesis is shown in Figure 1.

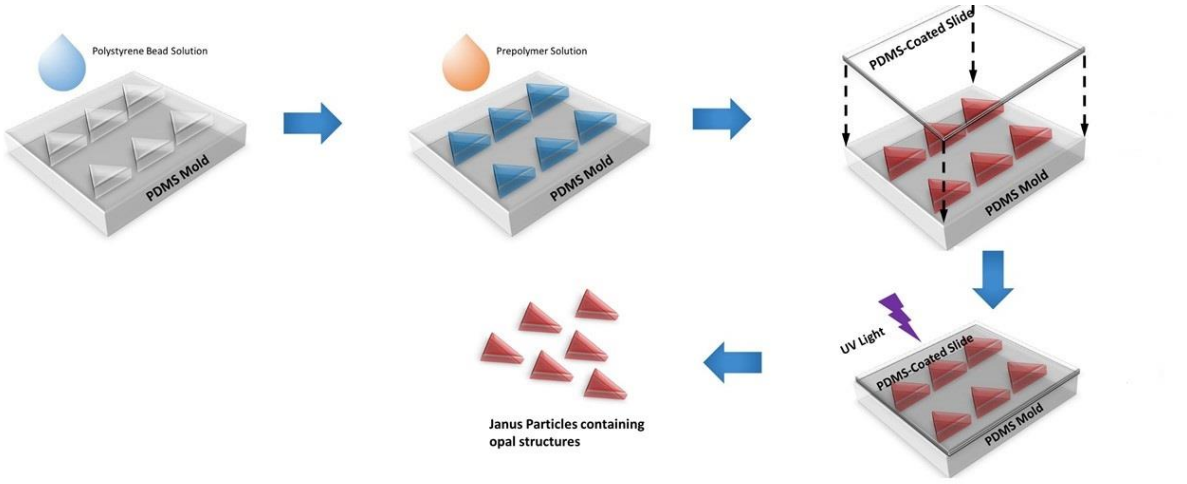

Figure 1: *Two-step micromolding technique for opal structured hydrogel microparticles.*

Briefly, I created a polystyrene (PS) bead solution comprised of an aqueous PS bead solution, ethanol, and Tween 20 (TW20). This solution was deposited onto poly(dimethylsiloxane) (PDMS) microwells in a humidity-controlled chambers. Next, I prepared

a prepolymer solution comprised of each acrylamide and bisacrylamide or poly(ethylene glycol) diacryate (PEGDA), a photoiniator (PI), and deionized water. The micromold was placed into a vacuum chamber to allow the prepolymer solution to seep into microwells. After the excess solution was removed, the micromold was placed under a handheld UV lamp (365 nm) to allow for radical induced polymerization. The microparticles were then collected with deionized water.

A number of important parameters in the fabrication process were examined such as surfactant concentration, ethanol concentration, polymer system, and presence of acrylic acid. Determination of optimal conditions for these parameters led to intense and uniform structural color contained in hydrogel microparticles with high yield of microparticles having color. The results show that Tween 20 is required in the PS bead solution, and PEGDA with acrylic acid is also required in the prepolymer solution to achieve uniform and intense color. A modified Bragg's equation was also developed to show how PS bead diameter and effective refractive index affect the photonic band gap. The predicted values from this equation were shown to correlate well with the experimental results. These created microparticles have the potential to be used for reagentless biosensing applications in the future.

2. Background

2.1 Opal Structure

2.1.1 Natural Opals

Opals are naturally occurring gemstones that are comprised of $SiO_2 \cdot nH_2O$ which is silicon dioxide surrounded by a number of water molecules[15]. Normally, opals do not display any color, but they can produce intense colors when the spheres are well-ordered and of similar sizes[16].

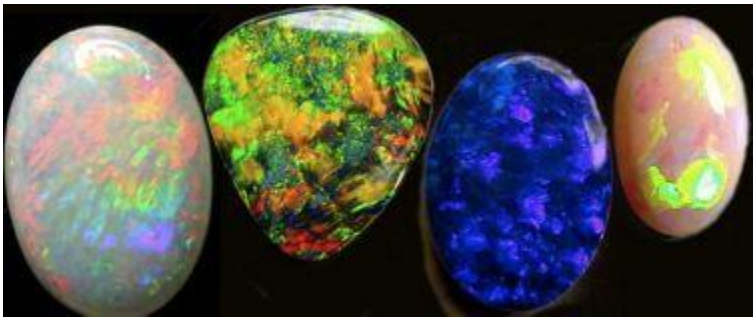

Figure 2: *Opal containing sections of bright color[16].*

This is a result of the light diffraction. The highly ordered sections of spheres refract white light at a single wavelength which gives rise to color which is not the result of any sort of pigment. The wavelength of light refracted is a result of the Bragg's equation[5]. The Bragg's equation states that the wavelength of the refracted light is a function of the spacing in between the spheres which in turn is related to the size of the spheres. This is how natural opals have regions of different color.

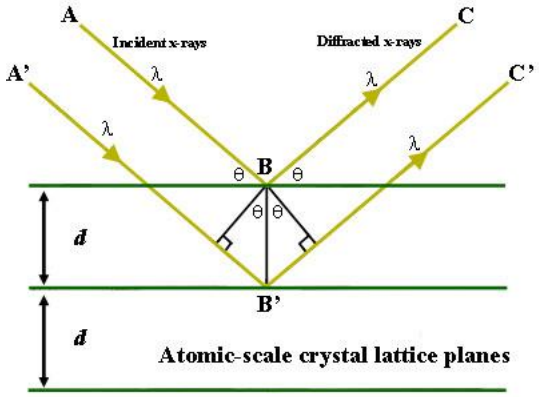

Figure 3: *Depiction of how light is refracted using Bragg's equation.*[17]

2.1.2 Synthetic Opals

In an attempt to replicate the brilliant structural color of natural opals, much has been done to synthetically fabricate nanoscale spheres that can be deposited into ordered structures. These ordered structures exhibit intense and uniform light. There have been many different materials utilized to create synthetic opal structures such as silica[1], polymers[2], or titanium[3]. When deposited these materials stack into face-centered cubic (FCC) structure. FCC structure is the most stable crystal packing since it is the most closely packed possible configuration[21]. The two most common methods for the deposition of nanoscale spheres into opal structures are self-assembly[22] and lithography[23]. Hydrogel microparticles containing opal structures fabricated via microfluidics have been shown to have been shown to undergo structural color change under different stimuli[30]. Stimuli observed have included pH, temperature[30], and organic solvents[31].

2.2 Polymeric hydrogels

Polymeric hydrogels are crosslinked networks of hydrophilic polymers[10]. Hydrogels have many potential applications in biosensing and medical diagnostics. This is a result of a number of desirable qualities of hydrogels. First off, hydrogels are biocompatible and nonfouling[12]. Hydrogels also have highly tunable properities[12] which can easily be controlled through the

modification of conditions such as monomer concentration and amount of a crosslinking agent present. Most importantly, hydrogels exhibit solution-like kinetics[12] due to which is a huge advantage over planar based assays. The 3D nature of hydrogels allows for very quick binding reactions. Due to these advantages, hydrogels have been utilized for a variety of applications ranging from drug delivery[25], to tissue engineering, to sensors[26]. Figure 4 shows hydrogel microparticles that have undergone a protein conjugation reaction. They are fluorescently labeled to demonstrate that the reaction has properly occurred. This was done to show the ability for the hydrogels to be utilized for biosensing.

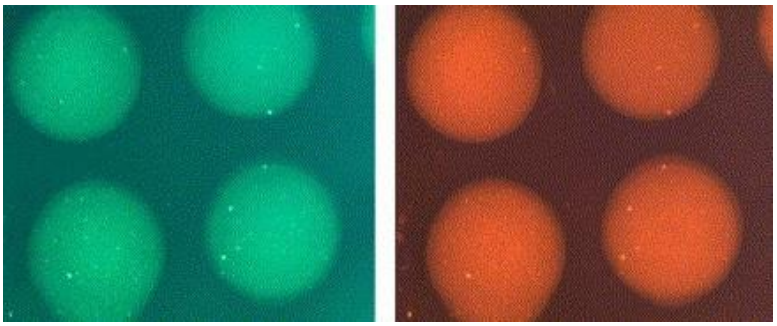

Figure 4: *Hydrogels being utilized for biosensing.*[27]

2.3 Fabrication techniques

There have been many developments into the production of consistent and uniform fabrication of hydrogels with microfluidic devices being the most commonly utilized method[11]. Microfluidics requires very precise control and manipulation of fluids on the microscale. To make hydrogels, microfluidics utilizes one laminar flow that contains a monomer and then utilizes a second flow to cause the monomer to make a desired shape. The monomer is then shone with harsh UV light to polymerize the monomer and form hydrogels. Microfluidics have been utilized to create hydrogels that contain opal structues[13,14].

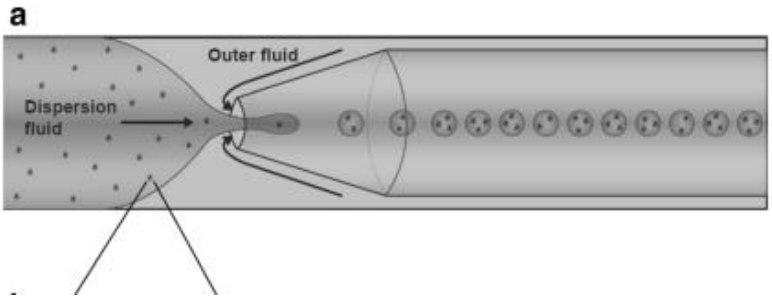

Figure 5: *Microfluidic fabrication of hydrogels*[28].

There are a number of issues with microfluidics that have led to the development of other technologies for the fabrication of hydrogels. These issues include harsh process conditions such as high intensity UV light, lack of scalability, and rapid polymerization required due to the short time that the hydrogels can be passed through UV light. Another method that has been becoming more popular is called the micromolding method[12]. Micromolding eliminates a number of the issues that were present in micromolding. Micromolding is scalable through parallelization, there is no requirement for harsh UV light, and polymerization can be done for any length of time so the type of polymers utilized is not as limited[10]. Micromolding works through the deposition of a monomer into microwells with equal volume followed by polymerization of the monomers. This allows for consistent fabrication of uniform hydrogels of various shapes and sizes. Opal structures currently have not been incorporated into hydrogels via micromolding.

3. Materials and Methods

3.1 Materials

Poly(ethylene glycol) diacrylate (PEGDA, average M_n 700 Da), 2-hydroxy-2-methylpropiophenone (Darocur 1173, photoinitiator (PI)), and acrylic acid (AA) anhydrous (180-200 ppm MEHQ inhibitor, 99%) were purchased from Sigma-Aldrich (St. Louis, MO). Acrylamide (AAm) (99.9%), Tween 20 (TW20), sodium dodecyl sulfate (SDS), and poly(dimethylsiloxane) (PDMS) elastomer kits (Sylgard 184) were purchased from Thermo Fisher Scientific (Waltham, MA). N,N'-Methylenebis(acrylamide) (Bis) was purchased from EMD Millipore (Billerica, MA). Ethanol (190 proof) was purchased from Decon Laboratories (King of Prussia, PA). Aqueous polystyrene (PS) bead solutions of varying diameters were fabricated by Mr. Jun Hyuk Lee in Professor Piljin Yoo's group at Sungkyunkwan University of Korea.

3.2 Fabrication of Janus Hydrogel Microparticles containing Opal Structures

First, polystyrene (PS) bead solutions were prepared by mixing aqueous solutions of PS beads of varying diameters, 20-70% v/v 190 proof ethanol, and either .01% v/v - .2% v/v TW20 or .1% w/v SDS by pipetting up and down in a microcentrifuge tube. PDMS micromolds were created through the thermal curing of Sylgard 184 elastomer with 10% w/v crosslinking agent following overnight incubation at 65°C on a silicon master template containing 40x40 square, circle, triangle, hexagon, or pentagon shaped microwells. The PS bead solution was then placed onto one of the 40x40 micromolds in a humidity-controlled chamber (~92% relative humidity). The solution was scratched into the microwells using a disposable pipette tip, and the excess PS bead solution was removed. The micromold was left in the humidity chamber to allow for the

chance for the PS beads to pack uniformly into crystal structures while the ethanol and water evaporated.

Next, a prepolymer solution was prepared containing either 15% total polymer (T) with a 4:1 ratio of acrylamide to bisacrylamide (AAm:Bis) and 1% v/v Darocur 1173 (PI) or 20% poly(ethylene glycol) diacrylate (PEGDA), 1% v/v PI, and 1% v/v acrylic acid (AA). The prepolymer solutions were mixed with a vortex mixer and sonicated for five minutes. The prepolymer solution was deposited onto the PDMS micromolds containing opal structures in the humidity-controlled chamber and then moved to a vacuum chamber. The micromolds were left in the vacuum chamber to allow the prepolymer solution to completely fill the microwells without disturbing the PS beads. After the microwells were filled, the micromold was removed from the vacuum chamber, put back into the humidity-controlled chamber, and the excess prepolymer solution was removed. A PDMS-coated slide with a small square cut out in the middle that is the size of the 40x40 square of microwells is placed onto the micromold to prevent evaporation of the prepolymer solution. The micromold is placed onto an aluminum mirror (Thorlabs, Newton, NJ), and 365 nm UV light from an 8 W hand-held UV lamp (Spectronics, Corp., Westbury, NY) was shown onto the micromold for 45 minutes for polyacrylamide (PAAm) or 15 minutes for PEGDA to initiate radical chain polymerization. The polymerized microparticles were collected by bending the PDMS mold and transferring them to a microcentrifuge tube with deionized (DI) water containing .05% v/v TW20. The microparticles were then cleaned at least three times with DI water containing .05% v/v TW20.

3.3 Optical Imaging Analysis

The Janus microparticles were imaged in DI water containing .05% v/v TW20 with an epifluorescence microscope (Olympus BX51 equipped with a DP70 microscope digital camera, Center Valley, PA) with either a 10x or 20x objective with light being shone down from the top of the microscope. Dimensions of the microparticles were determined using ImageJ analysis software[10] via the measure tool. The color uniformity of opal structures was determined by utilizing the particle analyzer in ImageJ.

4. Results and Discussion

4.1 Effect of ethanol concentration on the uniformity of polystyrene bead deposition and the color uniformity of the opal structures

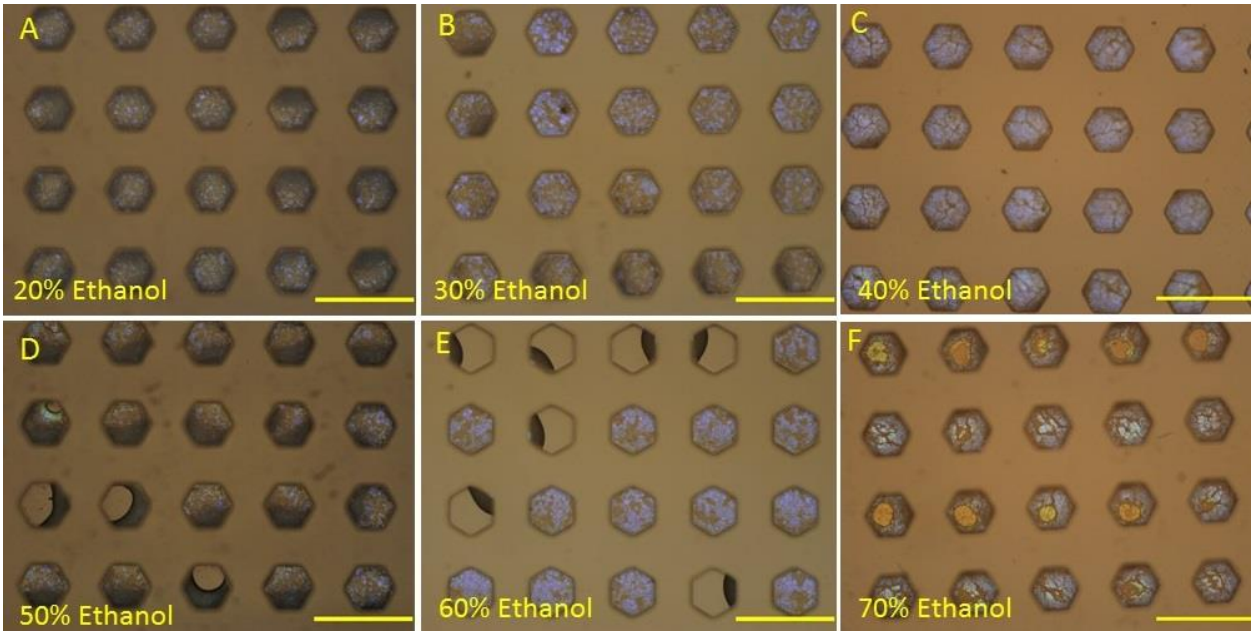

Figure 6: *Deposition of polystyrene beads onto PDMS micromolds with varying ethanol concentrations from 20%-70% v/v imaged with brightfield microscopy. Scale bars are 200 μm.*

First, I examined the effect of ethanol concentration on the uniformity of polystyrene (PS) bead deposition to determine an optimal concentration that leads to high levels of color uniformity. I hypothesized that mixing the aqueous PS bead solution with ethanol will lead to elimination of the meniscus that is present without ethanol that led to non-uniform packing (results not shown) and lead to more packing of the beads into face-centered cubic (FCC) crystal structure. All the conditions were tested in a humidity-controlled chamber to allow for the greatest chance for the PS beads to pack into FCC structure.

To test this hypothesis, I placed poly(dimethylsiloxane) (PDMS) micomolds in a humidity-controlled chamber with relative humidity of ~92%, and mixed an aqueous PS bead solution with varying amounts of ethanol. After deposition of particles and removal of the excess

solution, the microwells were slowly evaporated in the humidity controlled chamber. After drying, I imaged the microwells using top-down brightfield optical microscopy at 10x magnification and .1 second exposure time. The percentage of color uniformity was determined by examining the different colors present in each pixel on ImageJ. The particle analyzer was used to determine the amount of pixels with each different color within the microwells shown in the micrographs.

Figure 6A-C shows an increase in color uniformity as the ethanol concentration increases with 40% v/v ethanol having the highest amount of intense blue, uniform color with the percentage of pixels with blue color being 4.6%, 21.7%, and 75.4%, respectively. Figures 6D-F display the opposite trend with the amount of intense blue color decreasing as the ethanol concentration increases, and there are more microwells present that are not filled with an uniform layer of PS beads in the bottom of the well. For Figures 6D-F, the percentage of pixels with blue color are 18.3%, 72.9%, and 22.5%, respectively. The micrograph that has the highest amount of uniform blue color with very small amounts of brown and black color is Figure 6C. The micrographs with the least amount of color uniformity are Figure 6A and Figure6F. Figure 6A has very little blue color present and large amounts of brown and black color, and Figure 6F also has very little blue present with red and green spots.

There are two trends present that lead to a 40% v/v ethanol having the greatest amount of uniform structural color. The first trend is a direct relationship between color uniformity and ethanol concentration below 40% v/v ethanol, and the second trend is an inverse relationship between color uniformity and ethanol concentration above 40% v/v. At very low ethanol

concentrations, there is very little of the desired blue color present, and as ethanol concentration increases up to 40%, more uniform color emerges. Once 40% v/v ethanol is passed, the uniformity of the color present in the wells starts to decrease, and in some wells, the PS beads do not deposit in a layer across the bottom of the microwell. This suggests that ethanol concentration has an effect on the color uniformity of opal structures formed via deposition of the PS beads. The presence of ethanol may allow for more of the polystyrene beads to pack into face centered cubic (FCC) structure due to the elimination of the meniscus which is present in purely aqueous conditions. Regions with brown color are most likely contributed to the beads packing into simple cubic structure. However, as ethanol concentration climbs over 50% v/v, the wells appear to start to evaporate very quickly. This eliminates the chance for the PS beads to stack into FCC structure and decreases the amount of intense blue color. Also, increased evaporation prevents some of the microwells from being completely filled along the bottom with PS beads.

In summary, the results of Figure 6 demonstrate that the most effective concentration for the uniform deposition of PS beads is 40% v/v ethanol. This supports the hypothesis that adding ethanol eliminates the meniscus formation that prevents uniform packing, but too much ethanol causes there to be more non-uniform color.

4.2 Effect of surfactants on the uniformity of polystyrene bead deposition and the color uniformity of the opal structures

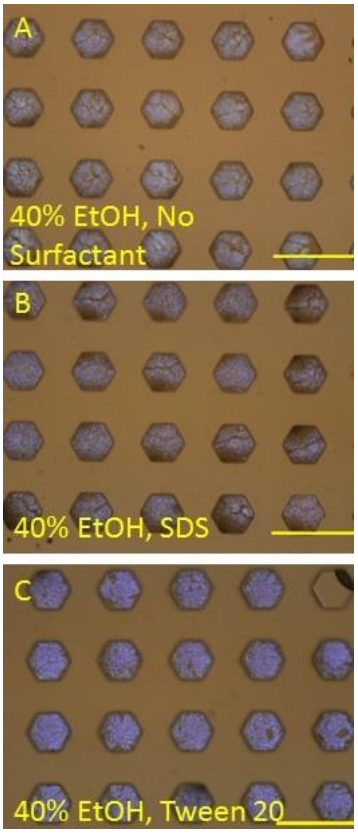

Figure 7: *Deposition of polystyrene beads to form opal structures imaged with top-down brightfield microscopy with (A) no surfactant and 40% EtOH, (B) .1% w/v SDS and 40% EtOH, and (C) .1% v/v Tween 20 and 40% EtOH. Scale bars are 200 μm.*

I next examined the effect of utilizing surfactant in the polystyrene bead solution in an attempt to increase color uniformity through an increase in packing uniformity. I hypothesize that using a surfactant will lead to an increase in color uniformity because the surfactant will lower surface tension at the air-water interface and allow for more uniform packing and therefore more uniform color since it appears that the PS bead solution is not evaporating completely uniformly which results in non-blue color. To test this hypothesis, I created a polystyrene bead solution comprised of three components: aqueous solution of polystyrene beads, 40% v/v ethanol

that was determined to achieve the highest amount of color uniformity, and .1% w/v SDS or .1% v/v Tween 20. I then followed the same procedure stated in section 4.1 to deposit the PS bead solution and image the microwells.

Figure 7a shows the level of color uniformity that was achieved with no surfactant. The micrograph in Figure 7b shows microwells where the polystyrene bead solution contained .1% w/v SDS. These micowells have more vibrant blue color, but there are many spots that are black and do not display any color with only 36.4% of the pixels displaying blue color determining by using ImageJ. This is an decrease from Figure 7a which is 75.4%. The third micrograph, Figure 7c, displays microwells where the polystyrene bead solution contains with .1% v/v Tween 20. The opal structures in the microwells exhibit highly uniform and intense blue color with only a few spots that are not blue. This micrograph had 86.3% of the area in the microwells displaying blue color.

The first surfactant I used in attempt to increase uniformity was sodium dodecyl sulfate (SDS). SDS did not appear to have a huge effect on the color uniformity which may be the result of the charge of the surfactant. This appears to disprove my hypothesis, but I think this lack of uniformity is not a result of surfactant properties. Sodium dodecyl sulfate is a negatively charged particle, and the polystyrene beads are slightly negatively charged. This leads to charge repulsion and prevents the polystyrene beads from packing uniformly into FCC structure. To remedy this, I tried using Tween 20 which is a neutrally charged surfactant instead of SDS. Using Tween 20 led intense, uniform color that was consistent across the large majority of wells. Tween 20 appears to not disrupt the packing of the polystyrene beads which can be seen in the increase in

color uniformity between the SDS and Tween 20 conditions, and allows for the polystyrene beads to evaporate more uniformly which leads to more uniform color.

In summary, Figure 7 confirms the hypothesis that a surfactant increases the uniformity of PS bead packing when the surfactant is nonionic. This increase in uniformity is most likely the result of the surfactant lowering the surface tension at the air-water interface which allows for uniform top down evaporation in the microwells.

4.3 Effect of surfactant concentration on the uniformity of polystyrene bead deposition and the color uniformity of the opal structures

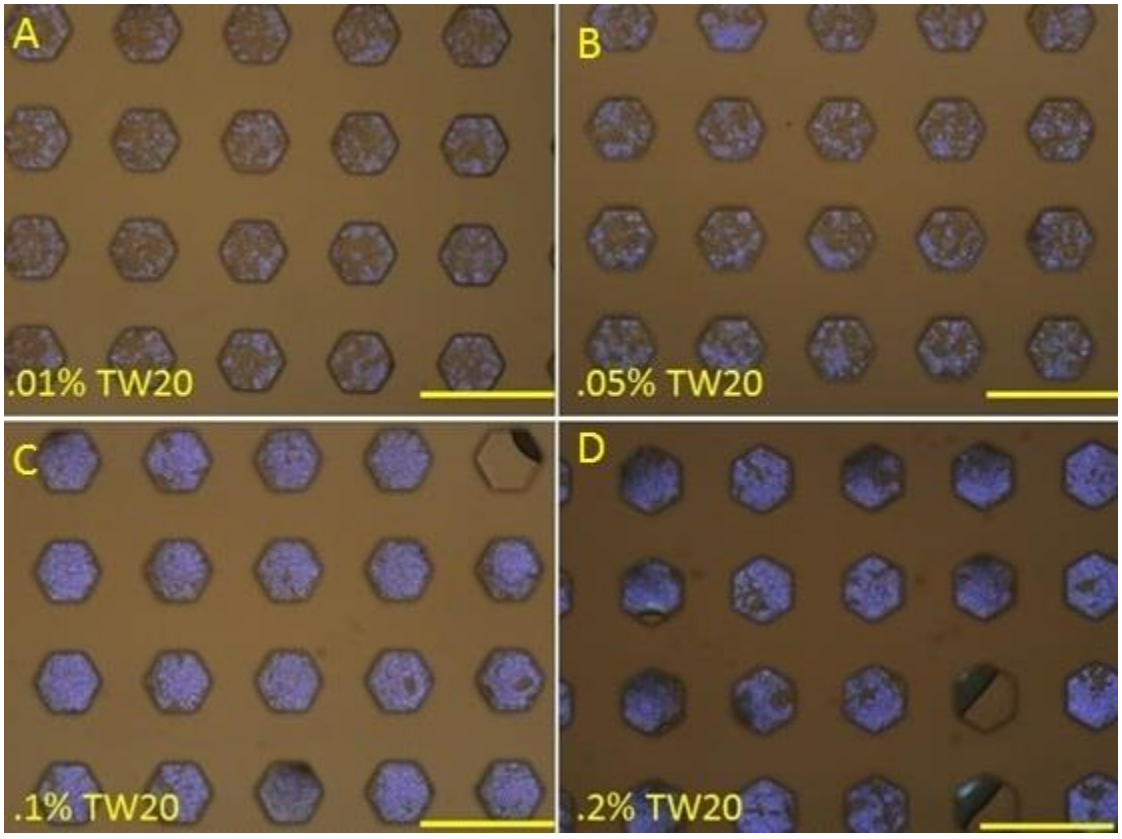

Figure 8: *Deposition of PS bead solutions containing 40% v/v EtOH with varying amounts of Tween 20 and imaged with top-down brightfield microscopy with (A) .01% v/v TW20, (B) .05% TW20, (C) .1% TW20, and (D) .2% TW20. Scale bars are 200 μm.*

With an ethanol concentration (40% v/v) and a type of surfactant determined (Tween 20), I next examined the effect of different Tween 20 concentrations on color uniformity of the created opal structures. I hypothesize that there is an optimal TW20 concentration that leads to the highest degree of color uniformity. I believe that as surfactant concentration increases, the surface tension at the air-water interface decreases, but eventually there is a lot of surfactant present not near the interface which interferes with packing.

To test this hypothesis, I prepared polystyrene bead solutions comprised of three components: 40% v/v ethanol, .01-.2% v/v Tween 20, and the remained aqueous polystyrene beads. I deposited the solution onto PDMS micromolds in a humidity controlled chamber at ~92% relative humidity. Once the excess solution was removed, I left the microwells to evaporate completely in the chamber. I imaged the microwells using top-down brightfield optical microscopy. The first two micrographs in Figure 8, Figures 8A and 8B, show very little blue color. The micrographs shown in Figures 8C and 8D both have portions of intense blue color, with structures in 8C giving rise to uniform blue color whereas structures in 8D lacking uniformity with many black spots present.

Figure 8 demonstrates that there is an optimal Tween 20 concentration for uniform color and packing of polystyrene beads into FCC opal structures. This optimal condition is .1% v/v Tween 20 where the color uniformity is 86.3%. Low concentrations of Tween 20 most likely do not have enough surfactant present to adequately lower the surface tension at the liquid-air interface which can be seen in the .01% v/v condition. Figures 8A and 8B have only 15.2% and 22.4% uniform blue color, respectively. As surfactant concentration increases, the surface tension lowers more and leads to more uniform packing via uniform top-down evaporation in the microwell. This can be seen from the increase in the presence of blue color in the .01%, .05%, and .1% v/v conditions. Once .1% v/v Tween 20 is reached, there is enough surfactant present to lower the surface tension to the point where uniform evaporation is present throughout the entire microwell. This leads to uniform and intense blue color which is consistent from microwell to microwell and from batch to batch. Above .1% v/v Tween 20, there is a decrease in the color uniformity of the formed opal structures. Figure 8D had 55.2% color uniformity, a sizeable

decrease from 86.3%. This effect may be the result of Tween 20 interfering with the packing of the polystyrene beads. At high concentrations, there is a lot of Tween 20 present in the polystyrene bead solution. Due to the relatively large size of Tween 20 and the fact that Tween 20 will aggregate to form micelles, Tween 20 may interfere with the packing of the PS beads. This leads to a decrease in color uniformity of the opal structures and prevents the beads from packing into FCC structure. This can be seen due to the presence of black and brown spots in the microwells.

Figure 8 demonstrates that .1% v/v Tween 20 leads to the highest degree of uniformity in packing of polystyrene beads into FCC structure. This is likely result of Tween 20 lowering the surface tension at the air-liquid interface. However, above .1% v/v Tween 20, it is possible that not all of the surfactant can align at the surface which can lead to a disruption of the packing of the polystyrene beads.

4.4 Effect of different sized polystyrene beads on the structural color of the formed opal structures

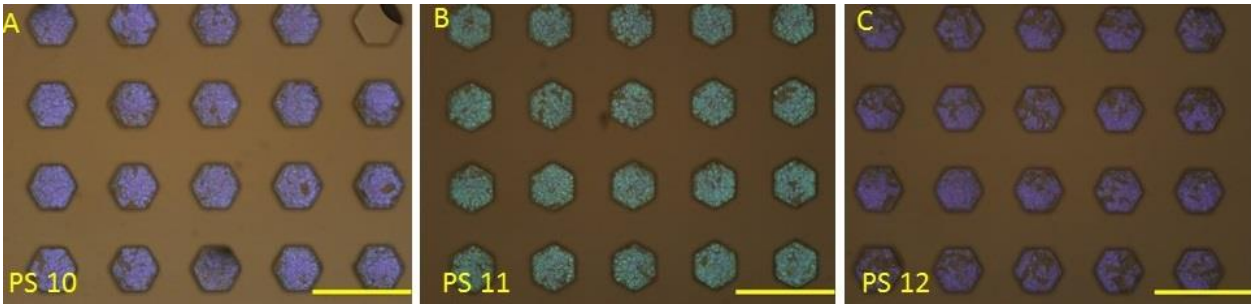

Figure 9: *Deposition of different aqueous polystyrene bead solutions mixed with 40% v/v EtOH, .1% v/v TW20 and imaged with top-down brightfield microscopy. The three different batches are (A) PS10, (B) PS11, and (C) PS12. Scale bars are 200 μm.*

With a set of conditions that lead to reliable and consistent formation of opal structures comprised of PS beads with intense and uniform color, I explored the effect of the changing the diameter of the PS beads being utilized to form opal structures. The three different batches of PS beads were fabricated by Mr. Jun Hyuk Lee in Professor Piljin Yoo's group at Sungkyunwan University in Korea. These batches were each synthesized via bulk polymerization utilizing different parameters in an attempt to create differently sized polystyrene beads.

To investigate this effect, I created different polystyrene bead solutions from thee three different aqueous polystyrene bead solutions. These aqueous solutions were mixed with ethanol and Tween 20 to reach concentrations of 40% v/v and .1% v/v, respectively. These bead solutions were then deposited and allowed to evaporate on PDMS micromolds in a humidity-controlled chamber with ~92% relative humidity. Afterwards, the microwells were imaged using top-down brightfield microscopy.

Figure 9A shows evaporated polystyrene beads from an aqueous stock solution that will be referred to as PS10. These beads display bright and intense blue color with 86.3% color uniformity. Figure 9B shows deposited polystyrene beads from a stock solution that will be referred to as PS11. The structural color of these beads were a teal color that is between blue and green. The color is both uniform and vibrant in the microwells with 81.5% color uniformity. Figure 9C shows polystyrene beads from a solution that will be referred to as PS12. These microwells have intense, uniform purple color with 67.3% color uniformity.

Each of the three micrographs in Figure 9 show a different color and the only difference between each of the experiments is the type of polystyrene bead solution being used. The microwells are imaged under the same fabrication conditions with the only difference between each micrograph being the different sized polystyrene beads. Because of this, the difference in the structural color of each image must be of the diameter of the polystyrene beads. Since the Bragg's equation states that the wavelength refracted from these opal structures is directly related to lattice spacing, and lattice spacing is directly related to particle diameter, the relative size of each of the polystyrene beads can be determined. PS11 refracts light at the longest wavelength, so these beads are the biggest. PS10 follows in terms of size, and PS 12 is the smallest of the three different batches.

Figure 9 demonstrates the effect that different size polystyrene beads size has on the structural color of the opal structures that are formed when the polystyrene beads are deposited into PDMS microwells. This allows for a wide range of different structural colors to be achieved when the Janus microparticles are completely formed.

4.5 Effect of utilizing an acrylamide:bisacrylamide system on the structural color of hydrogel Janus microparticles

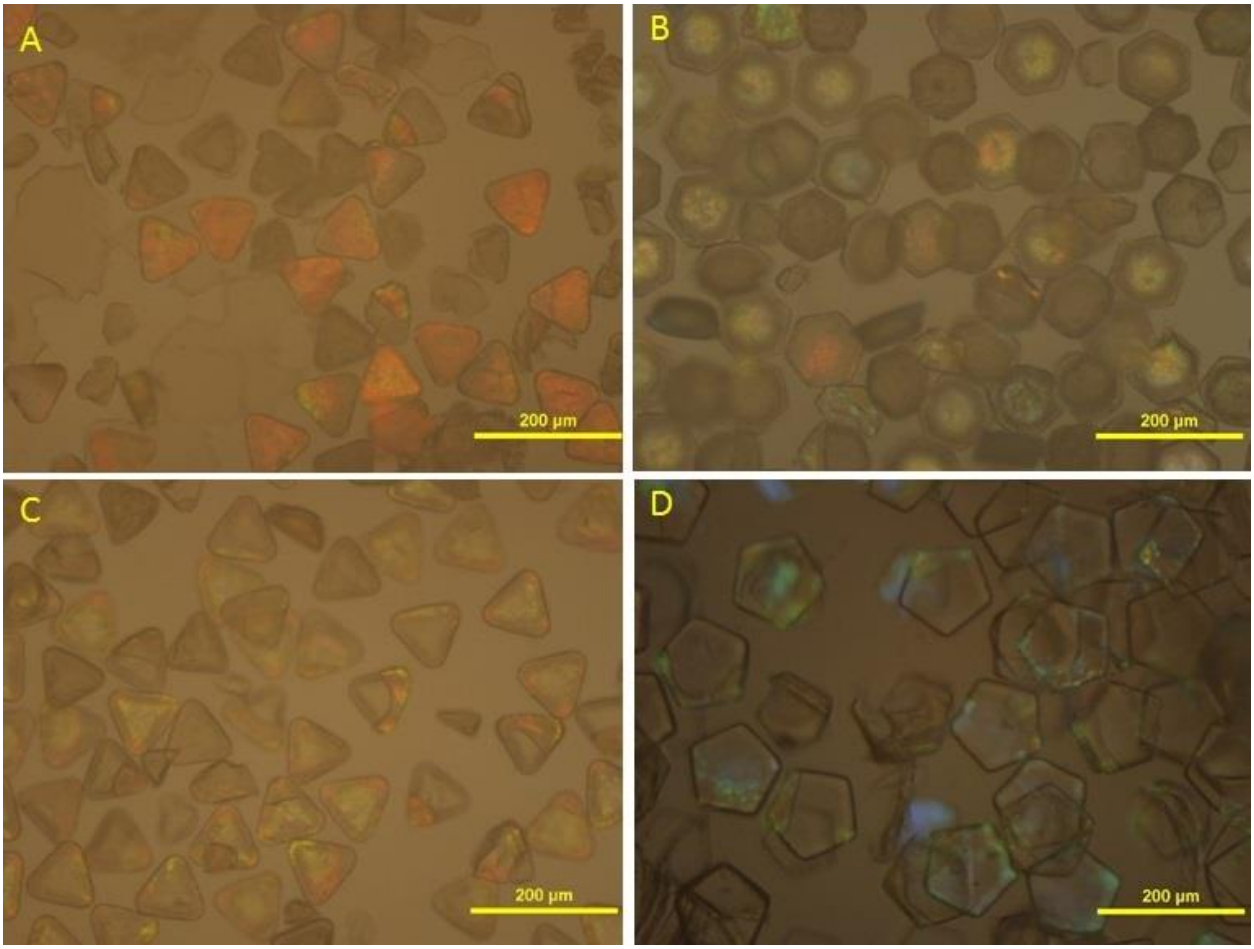

Figure 10: Top-down bright field micrographs of hydrogel Janus microparticles made from 15%T with 4:1 acrylamide:bisacrylamide with (A) highest yield that was achieved, (B) reoccurring problem of low yield of opal structure containing particles, (C) lack of uniform color within microparticles, and (D) both low yield of particles and non-uniform color.

With established conditions for formation of the first layer of the hydrogel Janus microparticles, I next tested the effect of utilizing an acrylamide:bisacrylamide (AAm:Bis) system for the second layer of the Janus microparticle. I hypothesize that the polyacrylamide (PAAm) system will lead to consistent fabrication of microparticles with high yields of particles containing opal structures with these particles having uniform and intense color.

To test this hypothesis, I created a polystyrene layer utilizing a polystyrene bead solution comprised of 40% EtOH, .1% v/v TW20, and aqueous PS bead solution. The layer was created following the same procedure that has been previously decreased. I created a prepolymer solution comprised of 15% total polymer (T) with a 4:1 ratio of AAm:Bis and 1% Darocur 1173 (PI) to initiate the radical polymerization. Once the PS bead layer was created, I added the prepolymer solution on the top of a PDMS mold and put the micromold into a vacuum chamber. The vacuum allowed for the prepolymer solution to completely fill the microwells without disturbing the PS beads. After I allowed for adequate time for the solution to seep into the microwells, I removed the micromold from the vacuum chamber, removed the excess prepolymer solution, and polymerized the microparticles for 45 minutes. I then collected the microparticles using deionized water and imaged the particles using top down brightfield microscopy.

All of the micrographs in Figure 10 are different batches of microparticles created with the same fabrication conditions as previously stated. Figure 10A shows a batch of microparticles with a yield of particles containing opal structures of about 50%. The color of the particles is red, and the color is very uniform within a single particle. There are also some particles that have broken apart and some that do not display any color. Figure 10B shows PAAm particles that have little to no color due to opal structures. There is a high yield of formed particles that are collected from the microwells, but there is an extremely low yield of particles containing opal structures. In the few particles that have color, the color is neither uniform nor intense. Figure 5\10C shows PAAm Janus microparticles. The yield of particles that contain opal structures is quite high, but the particles do not display uniform color. The particles display both yellow and

red color, and the color is not as intense as in the opal structures before polymerization. Figure 10D shows PAAm microparticles with the majority of these microparticles containing some color, but the color is not uniform within the particle. The particles have blue and green color mostly concentrating on the edge of the particles with some color present in the middle of the particles as well.

All of the micrographs in Figure 10 display microparticles with the same exact fabrication conditions. However, none of the images display the same structural color as each other, the structural color of the microparticles is not consistent, and there is generally low yields of microparticles with color. This demonstrates the amount of inconsistency that occurred in making microparticles with an AAm:Bis system. For the microparticles to be used for applications in the future, the particles need to have consistent and uniform color within a single particle, each batch of particles must have a high yield of microparticles containing opal structures, and the structural color needs to be the same from batch to batch. Since PAAm did not give any of these desired results, I determined that a different polymer system would need to be utilized and my hypothesis was disproved. This lack of consistency may be attributed to the long polymerization time of PAAm. During the polymerization, there is time for the acrylamide to disrupt the opal structures which eliminates the color. The lack of color might also be a result of the prepolymer not being able to completely fill the void in between the polystyrene beads. Then when the particles are removed, the polystyrene beads are left behind and the particles contain little to no opal structures. This could also account for the lack of intensity of color in many microparticles, since less layers of PS beads will result in less intense color.

In conclusion, I determined that an AAm:Bis system does not produce Janus microparticles containing opal structures with sufficient color uniformity and intensity. Another polymer system is needed to produce better results.

4.6 Effect of utilizing a PEGDA system on the structural color of hydrogel Janus microparticles

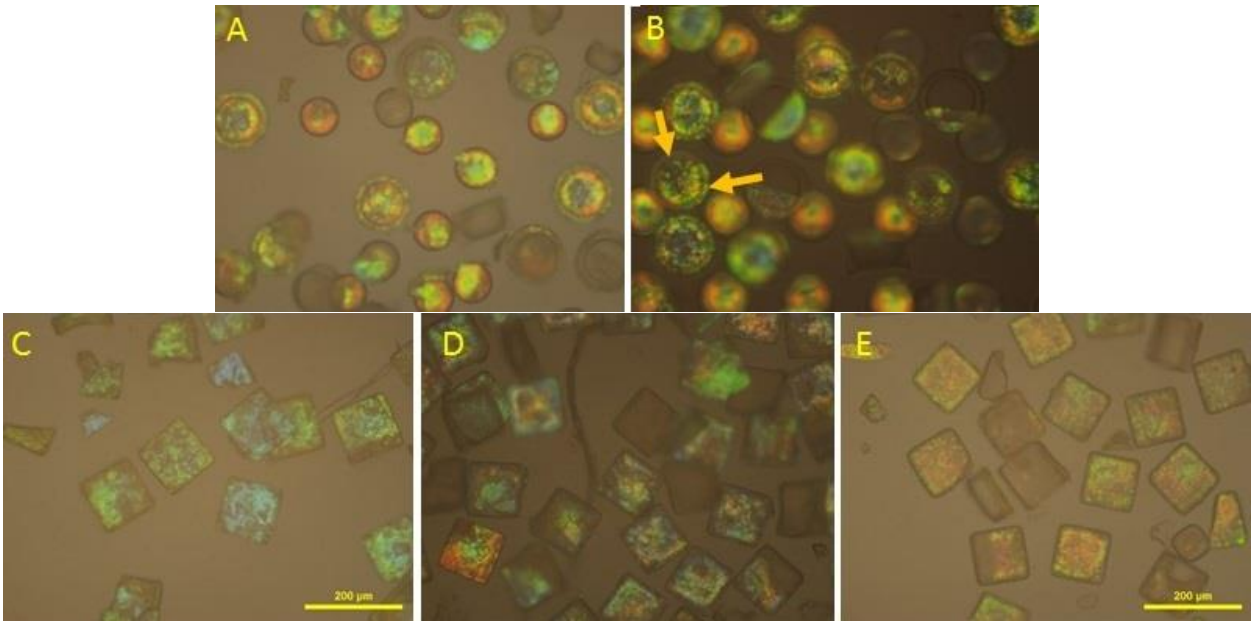

Figure 11: *Top-down brightfield micrographs of Janus microparticles made from 20% PEGDA in top row and microparticles fabricated from 20% PEGDA and 1% AA in the bottom row. Scale bars are 200 µm.*

With the inconsistencies that resulted from the PAAm system, I next utilized a poly(ethylene glycol) diacrylate (PEGDA) system to overcome those inconsistencies. I hypothesize that PEGDA will lead to more consistent and uniform results due to the shorter polymerization time and PEGDA interacting more favorably with the PS beads.

I created the polystyrene bead layer using a solution of PS beads containing 40% v/v EtOH and .1% v/v Tween 20. The deposition of the beads was done in the same method as previously described. I then created a prepolymer solution containing 20% v/v PEGDA, 1% PI, and either none or 1% v/v acrylic acid (AA). This prepolymer solution was deposited via vacuum chamber, and then the micromold was subjected to UV light for 15 minutes. I collected the

formed microparticles with deionized water and imaged the microparticles using top down brightfield microscopy.

Figures 11A and 11B are micrographs of PEGDA microparticles without acrylic acid with high yields of particles displaying structural color, but the color is not uniform within the particles. The color of the particles varies from red to yellow to green within a single particle. As can be seen by the arrows in Figure 11B, there is clear phase separation that occurred in almost all of the microparticles. This phase separation is caused by polymerization[12], and leads to the particles have different color in the different regions of the particle. Figures 11C, 11D, and 11E show micrographs of PEGDA microparticles that contain 1% AA. Figure 11C contains opal structures created from PS12 beads. These particles have blue/green uniform color with a very high yield of particles containing opal structures with 53.5% green color uniformity. Figure 11D shows microparticles with opal structures created from PS10 beads. These particles display fairly uniform yellow/green color with a high yield of particles containing opal structures with 41.2% yellow color uniformity. Figure 11E is a micrograph that shows microparticles where the opal structures were created from PS11 beads. These particles display uniform yellow/orange color with a high yield of particles displaying color with 43.5% orange color uniformity. This decrease in color uniformity shows that polymerization disrupted some of the opal structures and lowered the overall amount of uniformity in each particle.

When initially choosing a polymer to use, I choose to use PAAm because it does not undergo polymerization induced phase separation unlike PEGDA. This phase separation can clearly be seen in Figures 11A and 11B. Phase separation is not desired because it leads to

differences in structural color within a single particles. To combat this, I added acrylic acid to the prepolymer solution. I added acrylic acid to hopefully mitigate phase separation. As can be seen in the bottom three micrographs, AA led to a decrease in phase separation. These microparticles have fairly uniform color, and the yield of the particles containing opal structures is high. These results are also consistent from batch to batch, so PEGDA appears to be a good polymer system for the consistent and uniform fabrication of hydrogel Janus microparticles containing opal structures. Figures 11C, 11D, and 11E further demonstrate the effect of different sized PS beads has on structural color. The color of the microparticles corresponds to the relative sizes of the polystyrene beads with the smallest beads (PS12) corresponding to color with the shortest wavelength, the middle beads (PS10) having the second shortest wavelength, and the largest beads (PS11) corresponding to the color with the longest wavelength. This allows for the creation of a variety of colors for particles containing opal structures.

In conclusion, a prepolymer solution containing PEGDA and acrylic acid appears to be an adequate polymer system that leads to the fabrication of microparticles containing opal structures that display uniform and intense color consistently.

4.7 Modification of the Bragg's equation to a more useful form for a PS bead opal structure system

The governing equation for the refraction of light through an ordered crystal structure is the Bragg's equation.

$$\lambda = 2d\sqrt{\kappa - sin^2\theta}$$

***Equation 1**: General Bragg's Equation*

In its most general form, the Bragg's equation is shown by equation 1[15,16]. This equation states that the wavelength of the diffracted light is a function is a function of the lattice spacing (d), the dielectric constant (κ), and the angle of the light shown on the crystal struggle relative to normal incidence (θ). The variable n in the equation is the order of diffraction which is equal to one in for all experiments since the refracted light that is seen is the photonic bandgap[17]. This equation does not have much use in this form since I am interested in the change in the observed color as a function of both PS bead diameter and the effective refractive index of the materials used.

To begin to modify this equation, I used the following equations to make substitutions into the general Bragg's equation:

$$\theta = 0 \text{ (2.1)}$$

$$\kappa = \kappa_{ps}\Phi + \kappa_{void}(1 - \Phi) \text{ (2.2)}$$

$$\kappa = n^2 \text{ (2.3)}$$

***Equation 2**: Evaluation of θ and κ to be substituted into Bragg's equation.*

First, I set theta equal to 0 since the light that is shone onto the FCC opal structures is normal to the (111) plane[18] I then defined the overall dielectric constant as a function of the

dielectric constant of polystyrene beads that form the opal structures times the packing factor (Φ) and the dielectric constant of the void between the spheres times (1-Φ). The atomic packing factor is defined as the volume percentage that the spheres in the crystal structure occupy. Lastly, the dielectric constant is directly equal to effective refractive index squared[19]. Substituting equations 2.1, 2.2 and 2.3 into equation gives the following equation:

$$\lambda = 2d\left(n_{ps}^2\Phi + n_{void}^2(1-\Phi)\right)^{1/2}$$

Equation 3: Partially modified Bragg's equation.

This is a more usable form of the Bragg's equation, but to directly plug in values into the equation the lattice spacing needs to be written as a function of the diameter of the polystyrene beads. This was done using the following equations:

$$d = \frac{a}{\sqrt{h^2+l^2+k^2}} \qquad (4.1)$$

$$a = \sqrt{2}D \qquad (4.2)$$

Equation 4: *Lattice parameter substitutions for Bragg's equations.*

The lattice spacing, or the space between planes, is a function of both unit cell length, a, and the miller indices of the plane (hkl). Since light passes through (111), h, k, and l are all equal to one. The unit cell length of FCC structure is defined by equation 4.2[19]. Substituting equations 4.1 and 4.2 into equation 3 and plugging the miller indices into the equation 4.1 gives the modified Bragg's equation:

$$\lambda = \left(\frac{8}{3}\right)^{\frac{1}{2}} D\left(n_{ps}^2\Phi + n_{void}^2(1-\Phi)\right)^{\frac{1}{2}}$$

Equation 5: *Modified Bragg's equation.*

With equation 5, it is easy to plug values into this modified form of the Bragg's equation to determine the wavelength of light refracted through opal structures. The first application of the

modified Bragg's equation was to determine what the diameters of each of the three different PS bead aqueous solutions that had been used. These results are summarized in Table 1.

Batch	Approximate experimental wavelength (nm)	Calculated Diameter (nm)
PS10	430	180
PS11	475	200
PS12	500	210

Table 1: *Approximate diameters of PS bead solutions determined using modified Bragg's equation.*

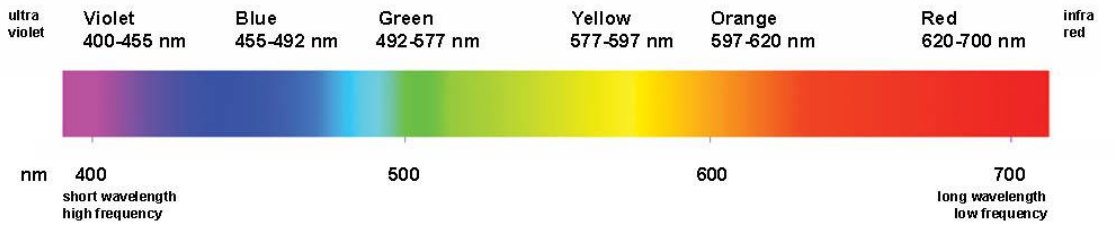

Figure 12: *Visible light spectrum and the corresponding wavelengths for each color*[29].

These experimental wavelengths were determined from the micrographs in **Figure 5** and the visible spectrum **in Figure 7 and** the following values were used for the effective refractive indices[20] : $n_{ps} = 1.59$ *and* $n_{void} = n_{air} = 1.0029$.

4.8 Examination of how diameter and effective refractive index change structural color and its relation to the modified Bragg's equation

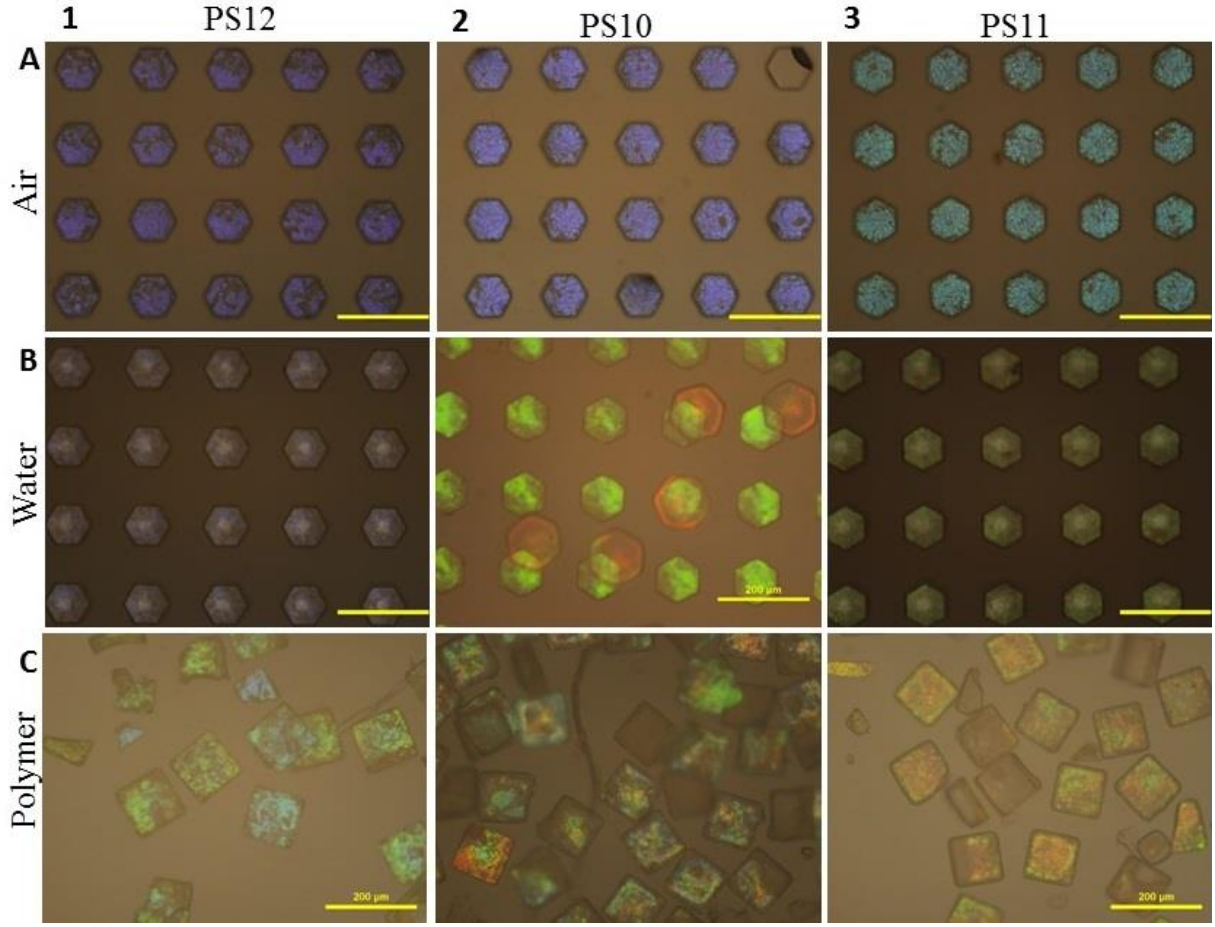

Figure 13: *Top-down brightfield micrographs of three different sized PS beads (PS11, PS10, and PS12 corresponding to columns 1, 2, and 3 respectively) under three different conditions. Row (A): Air, Row (B): Water, Row (C): hydrogel microparticles with 20% PEGDA and 1% AA. Scale bars are 200 µm.*

To test the veracity of the modified Bragg's equation, I subjected three different polystyrene bead solutions (PS10, PS11, and PS12) to three different conditions (air in the void between beads, water in the void, and PEGDA microparticles). This allows for nine different permutations of the two variables in the modified Bragg's equation (diameter and effective refractive index).

First, I deposited each of the three different polystyrene bead solutions containing aqueous polystyrene bead solutions, 40% v/v ethanol, and .1% v/v Tween 20 onto PDMS micromolds in a humidity-controlled chamber at ~92% relative humidity. The micromolds were then removed from the humidity-controlled chamber and imaged with top-down brightfield microscopy. Next, I pipetted deionized water on top of the micromold and imaged each of the molds again using top-down brightfield microscopy. After this, I created a prepolymer solution containing 20% PEGDA, 1% PI, and 1% AA. The micromold were placed into a vacuum chamber to allow the prepolymer solution to fill the microwells. I then put the micromolds under a UV lamp for 15 minutes, and then collected the microparticles with deionized water.

Column 1 of Figure 13 shows micrographs of PS12 beads with the void between beads being air for the first image, the void as water in the second image, and polymeric microparticles in the third image. The first micrograph shows uniform, intense purple color, and the second image shows a uniform blue/purple color. The particles have uniform green/blue color with a very high yield of particles containing opal structures. Column 2 of Figure 13 shows micrographs of microwells/particles containing PS10 beads. The first micrograph displays intense and uniform blue color. The second image displays intense, uniform green color, and the third image shows microparticles with fairly uniform yellow/green color. These microparticles have a high yield of particles containing opal structures. Column 3 of Figure 13 corresponds to micrographs of microwells or microparticles that contain PS11 beads. The first image displays microwells that have uniform teal color. The second image displays uniform green structural color. The third image displays microparticles with yellow/red color, and a high yield of particles containing opal structures.

The micrographs in Figure 13 demonstrate how the structural color of opal structures created from polystyrene beads shifts. When water is added onto a micromold to fill the void, all three different polystyrene bead solutions experience a red shift. This agrees with the modified Bragg's equation since the effective refractive index of water is greater than the effective refractive index of air. This relationship will be discussed in greater detail later. There is another red shift in the structural color when the microparticles are polymerized and collected in deionized water. This change in color is most likely the result of a slight change in refractive index due to some of the void being comprised partially of PEGDA, and an increase in lattice spacing due to swelling of the microparticles upon the addition of water. This also agrees with the relationship between lattice spacing and wavelength described in the Bragg's equation

Figure 13 demonstrates how the color of opal structures changes when both the effective refractive index and the lattice spacing of the opal structures change, and how these results agree with the relationships described in the modified Bragg's equation. To further explore this relationship, I used the approximate diameters of each PS bead solution to predict the wavelength for the water and microparticle conditions. All theoretical wavelengths were assigned an appropriate color from Figure 11**.** These results are summarized in Table 2.

		PS12	PS10	PS11
	Diameter (nm)	180	200	210
Air	Wavelength (nm)	430	475	500
Water	Wavelength (nm)	449	499	524
Particles	Wavelength (nm)	510	567	596

Table 2: *Predicted values for the wavelengths of three different sized PS beads in water and microparticle conditions*

The first set of predicted values is in the fourth row of Table 2. This corresponds to second row of Figure 13 where the opal structures were imaged in the presence of water. The effective refractive of water is equal to 1.33[20]. For the PS11 beads, the theoretical value was calculated to be 449 nm which corresponds to a blue color, and the experimental color is blue. For the PS10 beads, the theoretical value is 499 nm which is a green color, and the experimental color is green. The theoretical value calculated for the PS12 beads is 524 nm which corresponds to a green color, and the experimentally determined color was green. The theoretical values for this condition are similar to the experimental values with the difference in wavelength between the two most likely being a few nanometers.

Predicting the wavelengths for the Janus microparticles is more complicated than the first two conditions. This is due to the fact that I believe that color change is the result of both a change in the effective refractive index and a change in lattice spacing. When the microparticles are swollen in deionized water, the void in between the polystyrene spheres is a combination of both PEGDA and deionized water. To take this into account, I dried out microparticles (not pictured) with the same fabrication conditions of the particles in Figure 13 and determined their volume when swollen and after drying. With the volume determined when the microparticles were swollen with water and when there was no water present, I was able to calculate the percentage of the void occupied with water. I calculated this value to be 45%. This means that the void in between the polystyrene beads is 45% water when the microparticles are in deionized water. I then calculated an effective refractive index by doing a weighted average of the refractive index for water and refractive index for PEGDA. With $n_{PEGDA} = 1.47 \; and \; n_{water} = 1.33$, I calculated $n_{void} = 1.407$.

However, this does not account for all of the redshift in color that the microparticles display. To account for this, I think that the microparticles swell in deionized water, the lattice spacing of the PS beads increases as well. I again utilized micrographs of microparticles in deionized water and dried out microparticles (not pictured), to determine the degree of swelling. I calculated a degree of swelling by measuring the change in the length of the square microparticles before and after removing the water. I calculated the degree of swelling to be $D_s = 1.12$. I then plugged in the calculated effective refractive index into the modified Bragg's equation and then multiplied by the degree of swelling to take into account a bigger lattice spacing. These calculated values are in the fifth row of table 2. For PS12, the calculated value is 510 nm which corresponds to blue/green color, and the microparticles are blue and green. For PS10, the theoretical wavelength is 567 nm which corresponds to green/yellow color, and the experiment color is mostly yellow with some green. The theoretical wavelength for PS11 is 596 nm which is yellow and orange color, and the microparticles display yellow and orange color.

The experimental and theoretical colors agree with each other for all the different polystyrene bead batches. This shows that using degree of swelling to calculate the wavelength agrees with the data, but more tests needs to be done to determine if this is the actual mechanism that causes the shift in structural color. The modified Bragg's equation provides a useful tool that can be used to predict structural color for a variety of conditions.

5. Conclusion

In this thesis, I examined a number of different parameters that effect the fabrication of hydrogel Janus microparticles containing opal structures. I varied these parameters in the hope to achieve intense and uniform structural color. First, I focused on parameters that effect the deposition of PS into PDMS microwells. I found that mixing the aqueous PS bead solution with 40% v/v ethanol and allowing it to evaporate in a humidity-controlled chamber greatly improved the chance for the PS beads to pack into FCC structure. Next, I demonstrated that the addition of .1% v/v Tween 20 also improved the color uniformity of the opal structures through the lowering of surface tension without disrupting PS bead packing through charged molecules or presence of a large number of molecules. These conditions led to intense and uniform blue, teal, or purple color depending on the diameter of the PS beads. I also demonstrated that a polyacrylamide system for the hydrogel layer led to inadequate levels of color uniformity and consistency to be utilized due to structure disruption during polymerization. Instead, I determined that PEGDA is a promising polymer system when acrylic acid is added to help mitigate polymerization induced phase separation. This system leads to minimal disruption of opal structures due to short polymerization time. Finally, I derived a modified Bragg's equation that states the relationship between wavelength of refracted light and the diameter of the PS beads and the effective refractive index. I was able to use this equation to predict structural colors of opal structures that are very consistent with the experimental results. These results show the fabrication of uniform and intensely colored microparticles via sequential micromlding.

6. Future Directions

Although much progress has been accomplished in the fabrication of intense and uniform colored Janus hydrogel microparticles containing opal structures that has led to reliable results and high yields, there is more that needs to be done before the particles can be analyzed and potentially utilized for biosensing applications. PEGDA has been established as a very promising polymer system that leads consistent and uniform color, but additional conditions besides for the 20% PEGDA need to be tested and analyzed. Having a variety of PEGDA conditions that work will lead to a broader range of colors that can be achieved by a fixed diameter PS bead. The amount of acrylic acid present can also be varied to see more directly how it effects phase separation. This will lead to a better understanding of the microparticles which will be useful in the future.

One of the useful properties of including acrylic acid in the hydrogel layer is the carboxylate functionality that it provides. This property leads to swelling or shrinking when the pH changes, and this property can be utilized to observe how the structural color changes at different pHs. This will lead to a better understanding of how the degree of swelling affects structural color and will lead to more insight into how the modified Bragg's equation.

Finally, co-polymerization with either chitosan or acrylic leads to chemical functionalities that can be utilized to anchor probe biomolecules via bioconjugation reactions. These reactions can lead to changes in the effective refractive index that leads to a change in the structural color of the microparticles. This color changes allows for reagentless detection of binding events. These future studies will lead to a better understanding how the opal structures behave and how the microparticles can be utilized in the future.

7. References

[1] Blanco, A., Chomski, E., Grabtchak, S., Ibisate, M., John, S., Leonard, S. W., ... & Ozin, G. A. (2000). Large-scale synthesis of a silicon photonic crystal with a complete three-dimensional bandgap near 1.5 micrometres. Nature, 405(6785), 437-440.

[2] Zhang, J., Sun, Z., & Yang, B. (2009). Self-assembly of photonic crystals from polymer colloids. Current Opinion in Colloid & Interface Science, 14(2), 103-114.

[3] Liang, Z., Zheng, G., Li, W., Seh, Z. W., Yao, H., Yan, K., ... & Cui, Y. (2014). Sulfur cathodes with hydrogen reduced titanium dioxide inverse opal structure. ACS nano, 8(5), 5249-5256.

[4] Ge, J., & Yin, Y. (2011). Responsive photonic crystals. Angewandte Chemie International Edition, 50(7), 1492-1522.

[5] Lee, H. S., Kim, J. H., Lee, J. S., Sim, J. Y., Seo, J. Y., Oh, Y. K., ... & Kim, S. H. (2014). Magnetoresponsive discoidal photonic crystals toward active color pigments. Advanced Materials, 26(33), 5801-5807.

[6] Gajiev, G. M., Golubev, V. G., Kurdyukov, D. A., Medvedev, A. V., Pevtsov, A. B., Sel'kin, A. V., & Travnikov, V. V. (2005). Bragg reflection spectroscopy of opal-like photonic crystals. Physical Review B, 72(20), 205115.

[7] Dziomkina, N. V., & Vancso, G. J. (2005). Colloidal crystal assembly on topologically patterned templates. Soft Matter, 1(4), 265-279.

[8] Rhee, D. K., Jung, B., Kim, Y. H., Yeo, S. J., Choi, S. J., Rauf, A., ... & Yoo, P. J. (2014). Particle-nested inverse opal structures as hierarchically structured large-scale membranes with tunable separation properties. ACS applied materials & interfaces, 6(13), 9950-9954

[9] Shkunov, M. N., Vardeny, Z. V., DeLong, M. C., Polson, R. C., Zakhidov, A. A., & Baughman, R. H. (2002). Tunable, gap-state lasing in switchable directions for opal photonic crystals. Advanced Functional Materials, 12(1), 21-26.

[10] Liu, E. Y., Jung, S., & Yi, H. (2016). Improved Protein Conjugation with Uniform, Macroporous Poly (acrylamide-co-acrylic acid) Hydrogel Microspheres via EDC/NHS Chemistry. Langmuir, 32(42), 11043-11054.

[11] Chung, B. G., Lee, K. H., Khademhosseini, A., & Lee, S. H. (2012). Microfluidic fabrication of microengineered hydrogels and their application in tissue engineering. Lab on a Chip, 12(1), 45-59.

[12] Jung, S., & Yi, H. (2012). Fabrication of chitosan-poly (ethylene glycol) hybrid hydrogel microparticles via replica molding and its application toward facile conjugation of biomolecules. Langmuir, 28(49), 17061-17070.

[13] Gorey, B., Smyth, M. R., White, B., & Morrin, A. (2014). Fabrication of homogenous three dimensionally ordered conducting polymer–polystyrene opal structures in microfluidic channels. Journal of Materials Chemistry C, 2(30), 6004-6009.

[14] Gorey, B., Galineau, J., White, B., Smyth, M. R., & Morrin, A. (2012). Inverse-Opal Conducting Polymer Monoliths in Microfluidic Channels. Electroanalysis, 24(6), 1318-1323.

[15] Opal. (2017). In Encyclopædia Britannica. Retrieved from http://academic.eb.com.ezproxy.library.tufts.edu/levels/collegiate/article/opal/57166

[16] Opal (n.d.). Retrieved from http://www.webexhibits.org/causesofcolor/15F.html

[17] Bragg reflection spectroscopy of opal-like photonic crystals Phys. Rev. B. 72, 205115 (2005)

[18] Controlled tuning of the stop band of colloidal photonic crystals by thermal annealing Optical Materials. 32(9), 946-949 (2010)

[19] DoITPoMS. (2014). Retrieved from https://www.doitpoms.ac.uk/tlplib/dielectrics/dielectric_refractive_index.php

[20] Refractive Index Values. (n.d.). Retrieved from http://hyperphysics.phy-astr.gsu.edu/hbase/Tables/indrf.html

[21] Callister, W. D., & Rethwisch, D. G. (2016). Fundamentals of materials science and engineering: an integrated approach.

[22] Norris, D. J., Arlinghaus, E. G., Meng, L., Heiny, R., & Scriven, L. E. (2004). Opaline Photonic Crystals: How Does Self-Assembly Work?. Advanced Materials, 16(16), 1393-1399.

[23] Waterhouse, G. I., & Waterland, M. R. (2007). Opal and inverse opal photonic crystals: fabrication and characterization. Polyhedron, 26(2), 356-368.

[24] Anker, J. N., Hall, W. P., Lyandres, O., Shah, N. C., Zhao, J., & Van Duyne, R. P. (2008). Biosensing with plasmonic nanosensors. Nature materials, 7(6), 442-453.
[25] Appel, E. A., del Barrio, J., Loh, X. J., & Scherman, O. A. (2012). Supramolecular polymeric hydrogels. Chemical Society Reviews, 41(18), 6195-6214.

[26] Butun, S., & Sahiner, N. (2011). A versatile hydrogel template for metal nano particle preparation and their use in catalysis. Polymer, 52(21), 4834-4840.

[27] Yadavalli, V. K., Koh, W. G., Lazur, G. J., & Pishko, M. V. (2004). Microfabricated protein-containing poly (ethylene glycol) hydrogel arrays for biosensing. Sensors and Actuators B: Chemical, 97(2), 290-297.

[28] Easley, C. J., Karlinsey, J. M., Bienvenue, J. M., Legendre, L. A., Roper, M. G., Feldman, S. H., ... & Landers, J. P. (2006). A fully integrated microfluidic genetic analysis system with sample-in–answer-out capability. Proceedings of the National Academy of Sciences, 103(51), 19272-19277.

[29] Barney, C., Dich, A., & Koufos, D. (2014). VISIBLE LIGHT COMMUNICATION SYSTEMS. Worcester Polytechnic Insitiute.

[30] Wang, J., Hu, Y., Deng, R., Liang, R., Li, W., Liu, S., & Zhu, J. (2013). Multiresponsive hydrogel photonic crystal microparticles with inverse-opal structure. Langmuir, 29(28), 8825-8834.

[31] Zhao, H., Gao, J., Pan, Z., Huang, G., Xu, X., Song, Y., ... & Qiu, H. (2016). Chemically Responsive Polymer Inverse-Opal Photonic Crystal Films Created by a Self-Assembly Method. The Journal of Physical Chemistry C, 120(22), 11938-11946.